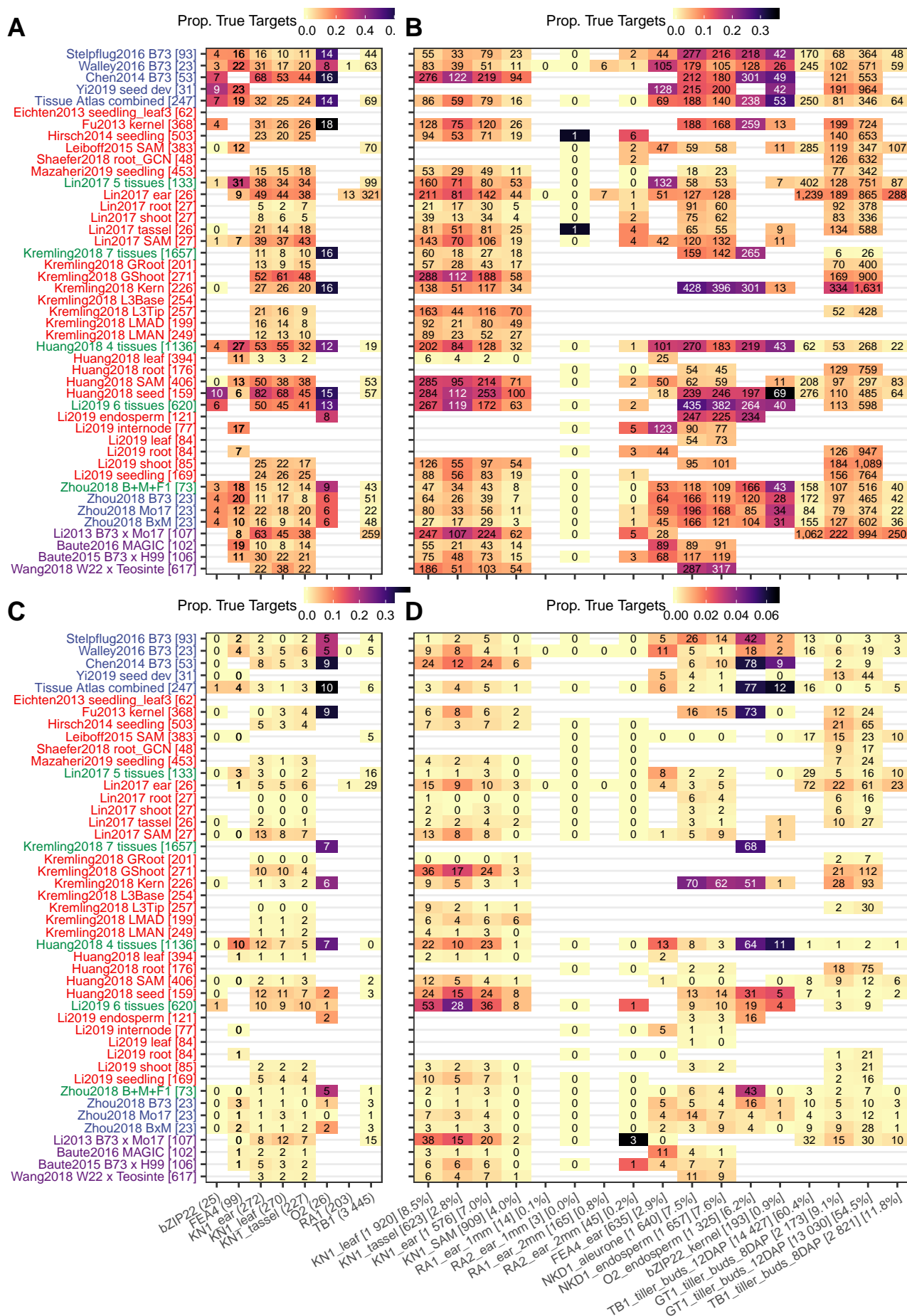
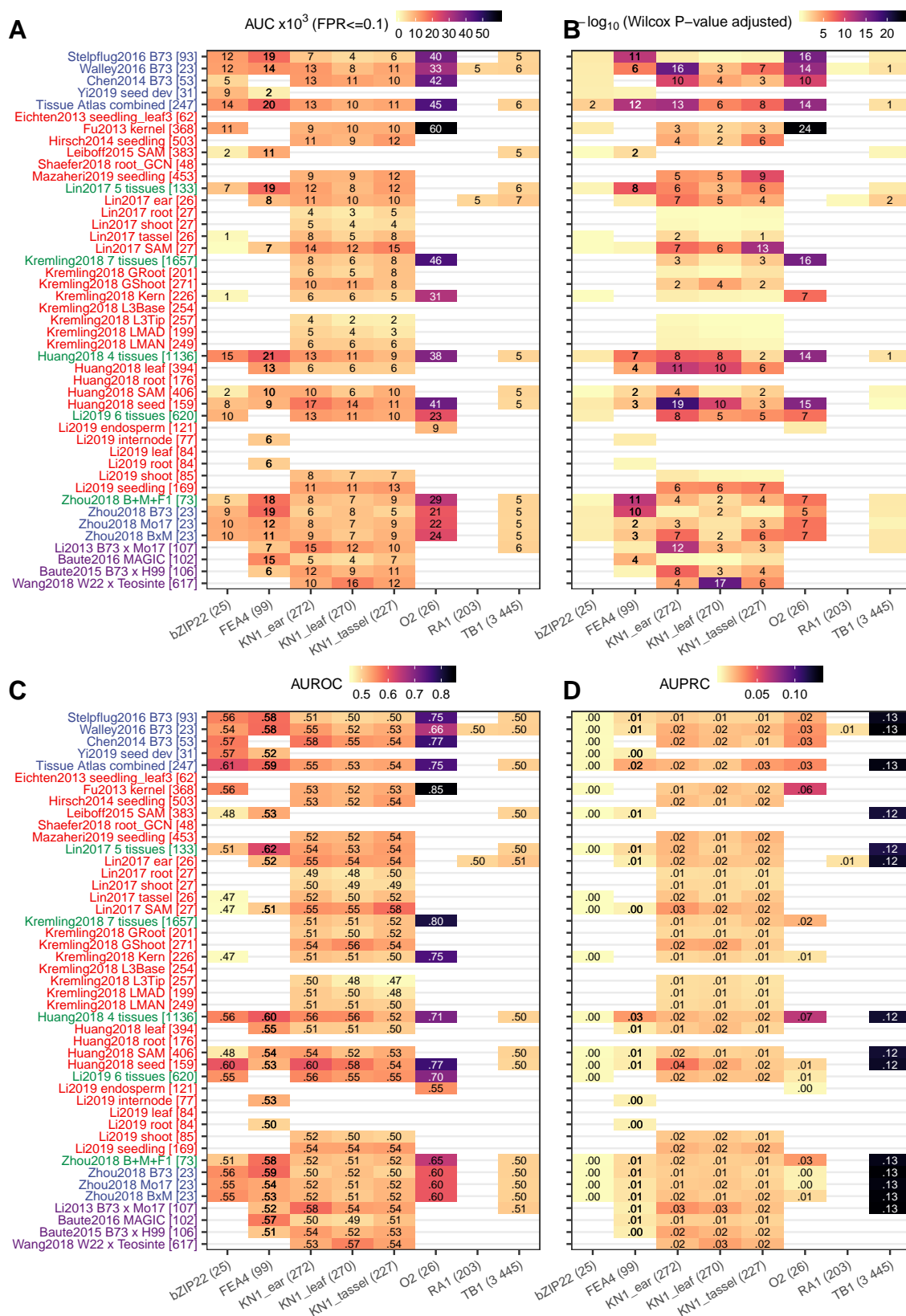


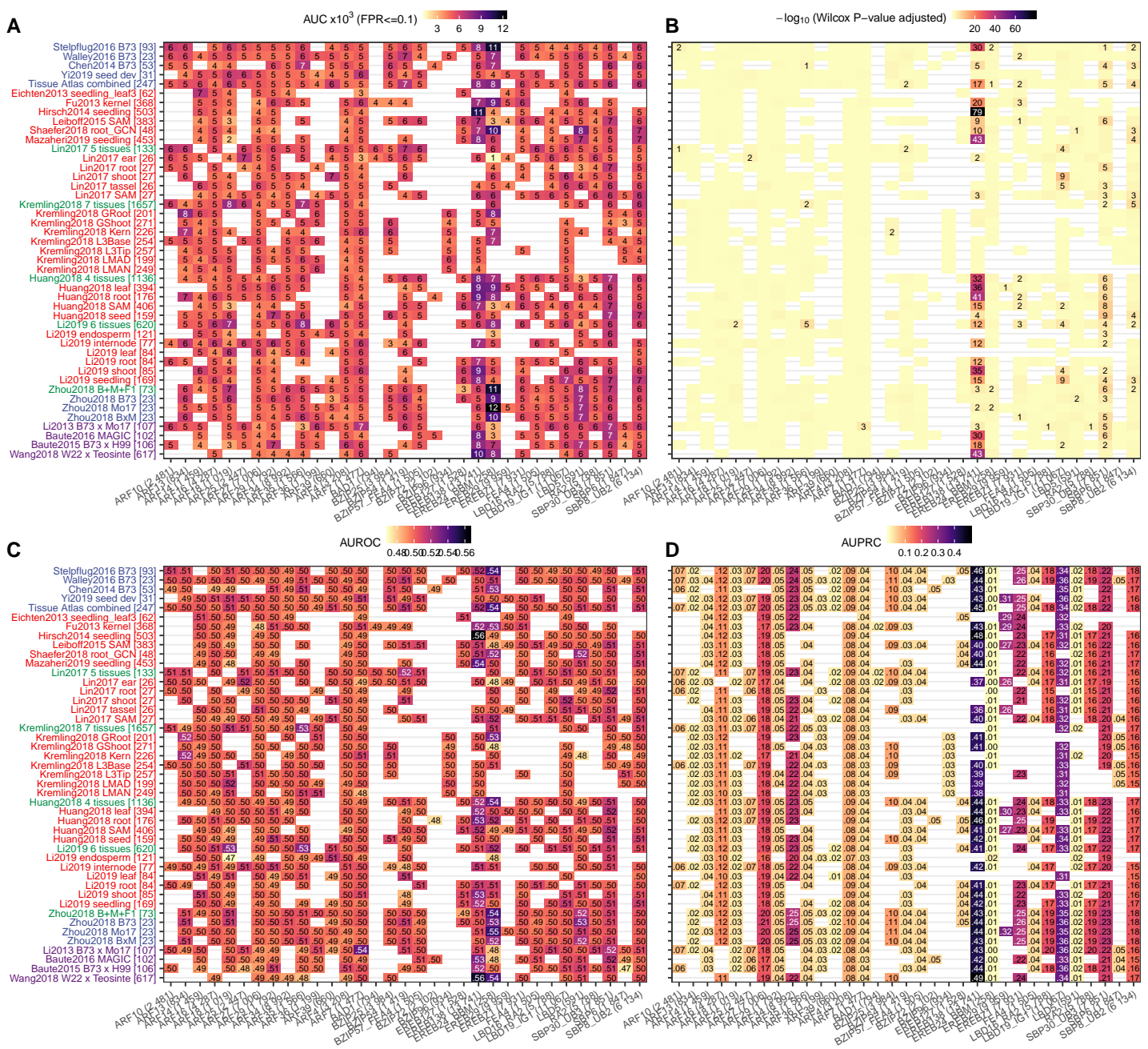
Supplemental Figure 1. Comparison of GRNs built using different methods according to the enrichment of functional annotations (Gene Ontology, CornCyc, and so on) (Supports Figure 2). For each network only the top 100,000 predicted TF-target associations were taken. Fold enrichment is calculated as the observed number of shared GO/CornCyc terms (by targets regulated by a common TF) divided by the expected number of shared annotation terms (determined by permutation). The names for each of the networks are color-coded to indicate B73 developmental surveys (blue), genotype surveys (red), meta-networks (green) or previously generated GRNs (teal). Each GRN was built using three regression methods: RF (random forest), ET (extra trees) and XGB (gradient boosting).

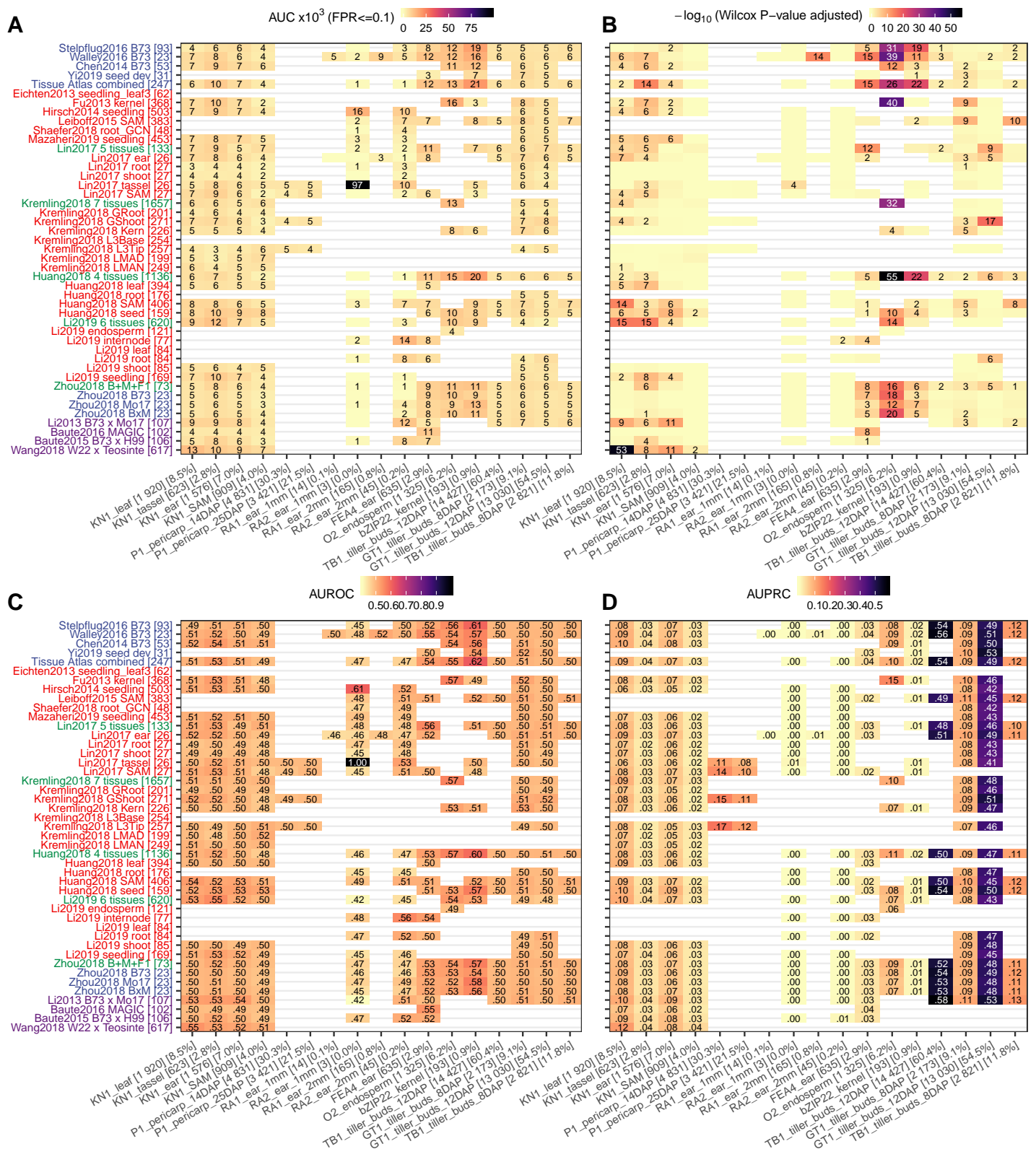


Supplemental Figure 2. Number of true TF targets captured by the top one million predictions and the top 100K predictions in each GRN (Supports Figure 2 and 3). (A) and (C): direct targets of published TF studies derived from ChIP-Seq and mutant RNA-Seq experiments; (B) and (D) For each one of the 17 maize TFs with knockout mutant RNA-Seq data available, differentially expressed genes between mutant and wildtype were identified using DESeq2 (p-value < 0.01). Numbers in each cell represent the actual number of true targets captured by each GRN during each evaluation, while cells were colored based on the proportion of captured true targets. Blank (white) cells stand for missing data where the TF being evaluated is not expressed or not variable (i.e., zero variance) in the corresponding GRN. Y-axis labels correspond to the different networks listed in Table 1. X-axis labels (e.g., “KN1_ear (272)” or “KN1_ear [1576] [7.0%]”) represent the common name for each TF, the tissue in which the TF is expressed, followed by the number of direct targets (Panels A and C) or number and proportion of differentially expressed genes in TF mutant (Panels B and D).

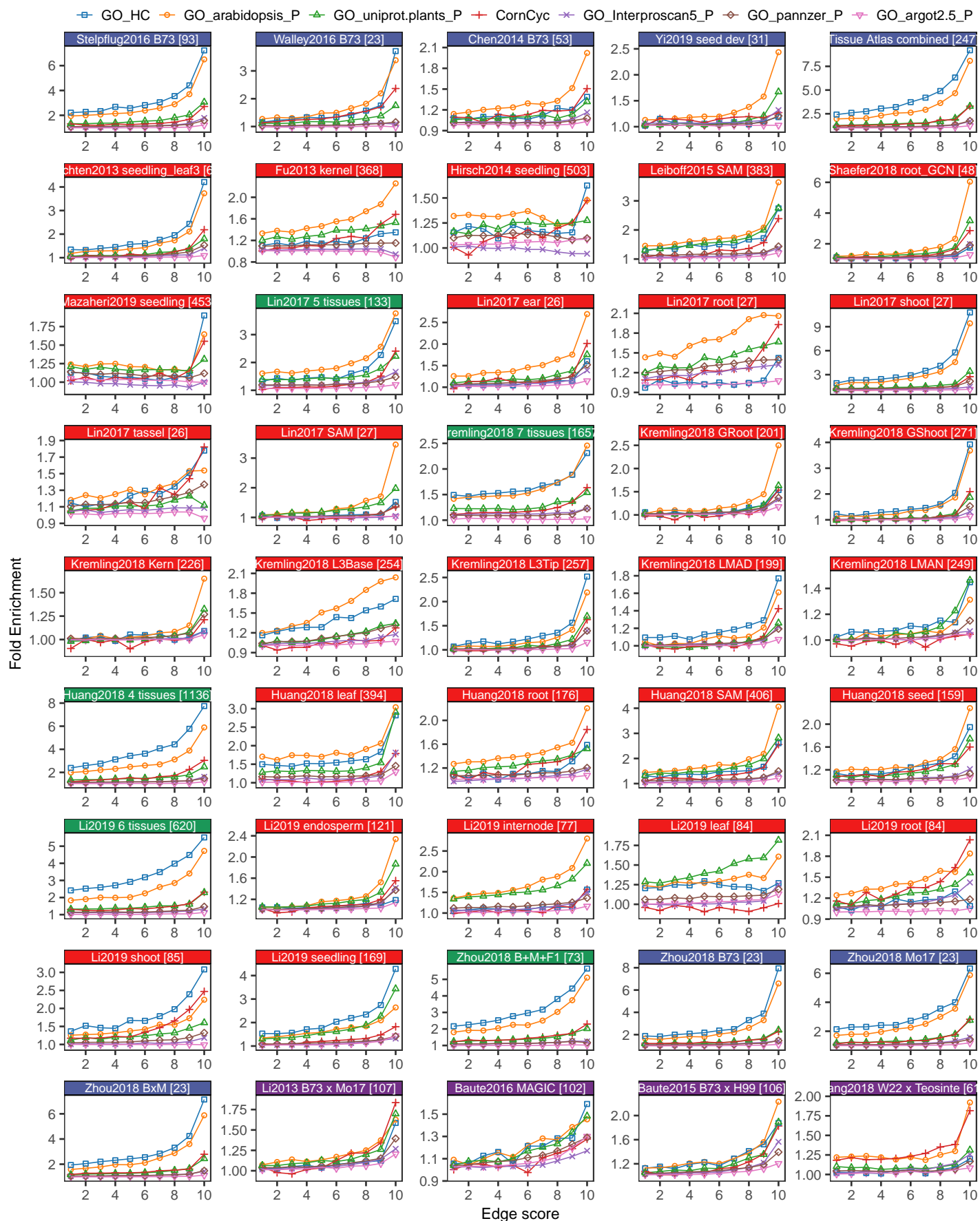


Supplemental Figure 3. Evaluation of GRNs using support from direct targets of eight known TFs (Supports Figure 2A). (A) Area under receiver-operating characteristic curve (AUROC) until an False Positive Rate of 0.1 is reached; (B) Wilcox rank test performed using the predicted (TF-target) interaction scores between the group of true targets (DEGs) and non-targets (non-DEGs); (C) Area under receiver-operating characteristic curve (AUROC) and (D) Area under precision-recall curve (AUPRC). Light yellow cells with no numbers stand for “not significant” ($P > 0.05$), while blank (white) cells stand for missing data where the TF being evaluated is not expressed or not variable (i.e., zero variance) in the corresponding GRN.



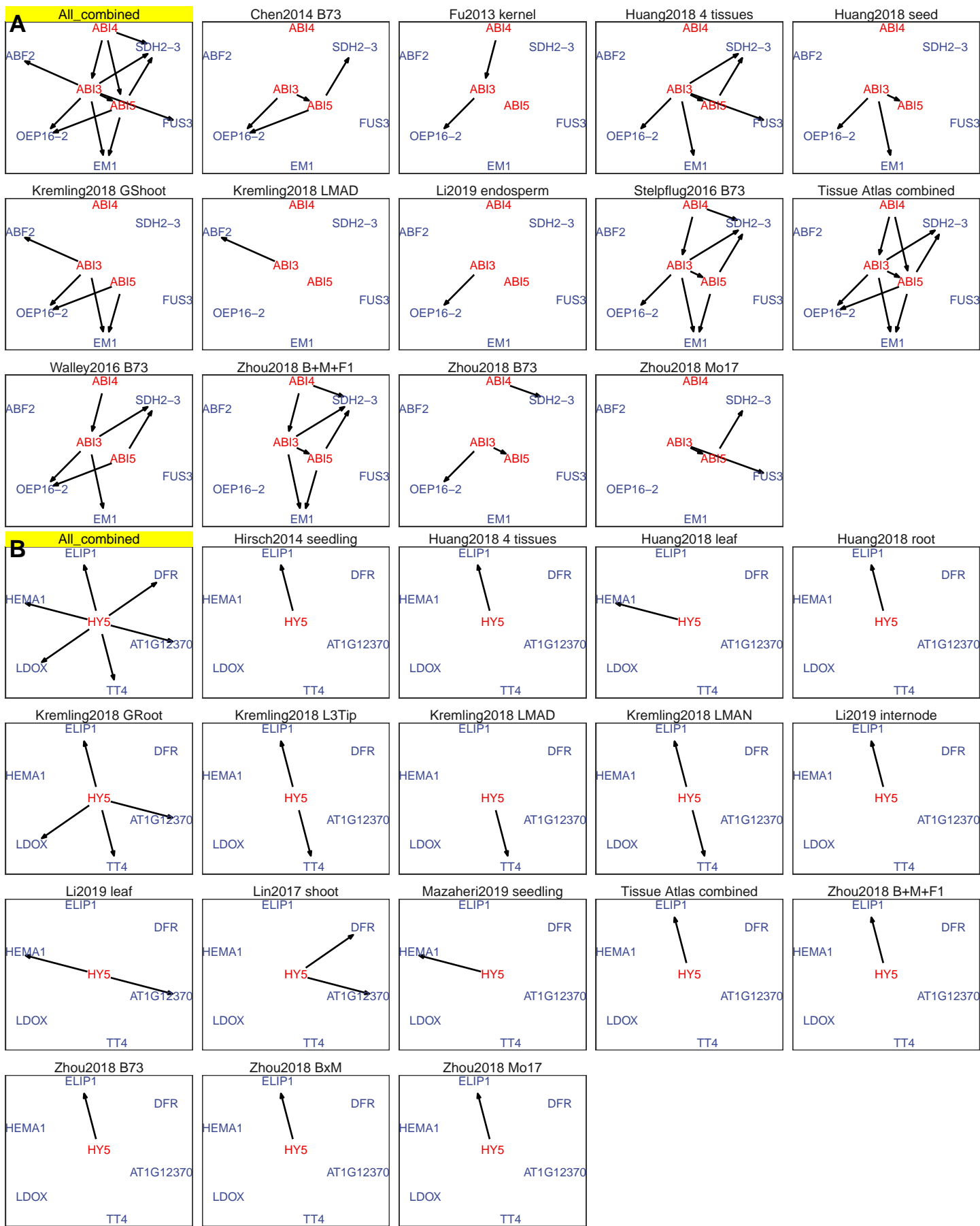


Supplemental Figure 5. Evaluation of GRNs using support from 17 maize TF knockout mutant RNA-Seq datasets (Supports Figure 2). (A) Area under receiver-operating characteristic curve (AUROC) until an False Positive Rate of 0.1 is reached; (B) Wilcox rank test performed using the predicted (TF-target) interaction scores between the group of true targets (DEGs) and non-targets (non-DEGs); (C) Area under receiver-operating characteristic curve (AUROC) and (D) Area under precision-recall curve (AUPRC). Light yellow cells with no numbers stand for “not significant” ($P > 0.05$), while blank (white) cells stand for missing data where the TF being evaluated is not expressed or not variable (i.e., zero variance) in the corresponding GRN.



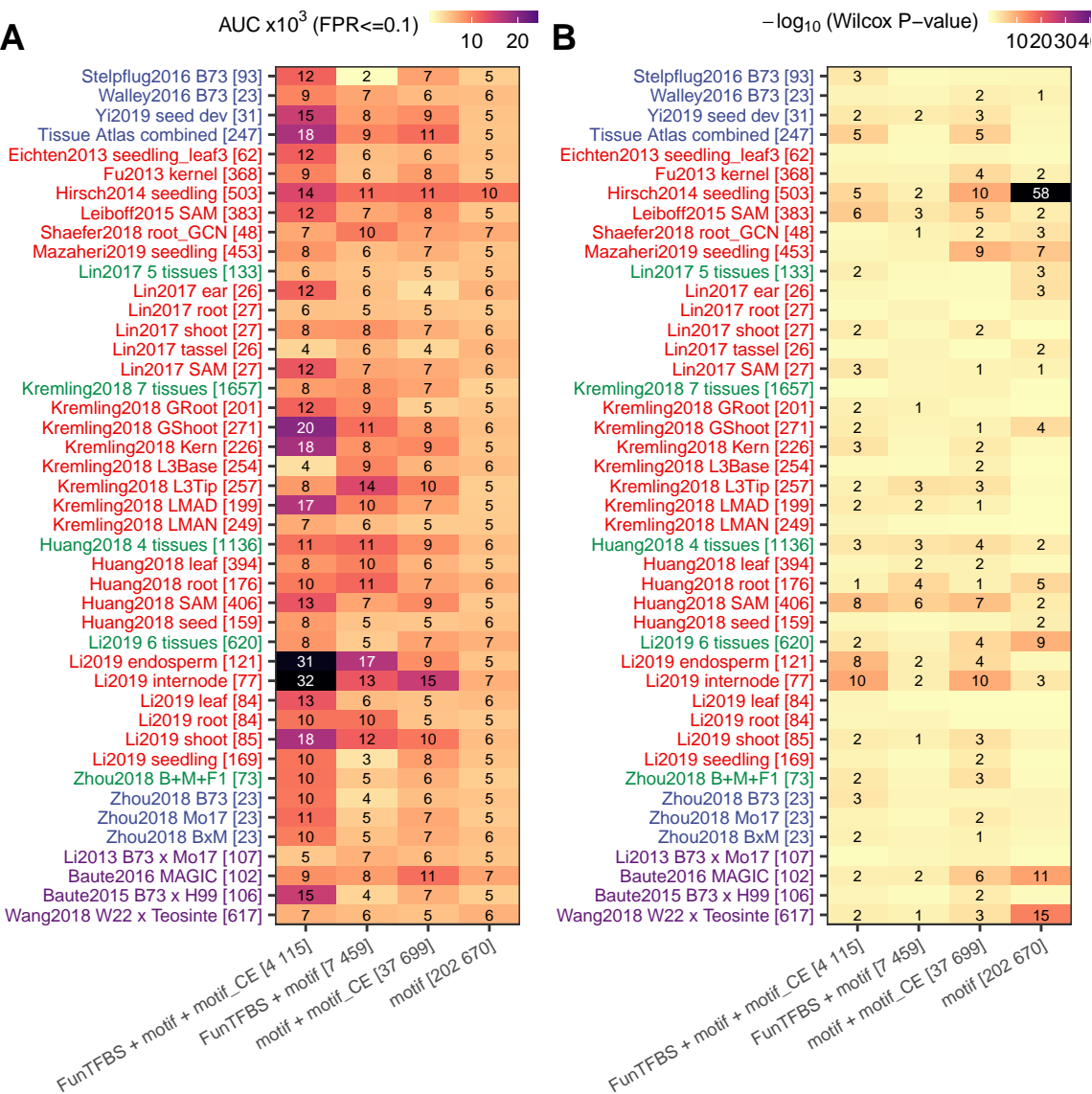
Supplemental Figure 6. Enrichment of co-annotated GO/CornCyc terms in co-regulated network targets (Supports Figure 3A). For

each network the top 1 million predicted TF-target associations were binned to 10 bins and assessed for enrichment of GO/CornCyc functional annotation. Fold enrichment is calculated as the observed number of shared GO/CornCyc terms (by targets regulated by a common TF) divided by the expected number of shared annotation terms (determined by permutation). The names for each of the networks are color coded to indicate B73 developmental surveys (blue), genotype surveys (red), meta-networks (green) or previously generated GRNs (teal). A total of six sources of GO annotation were used: GO_HC (high quality hand-curated terms transferred from maize AGP_v3 annotation), GO_arabidopsis, GO_uniprot.plants, GO_Interproscan5, GO_pannzer and GO_argot2.5.

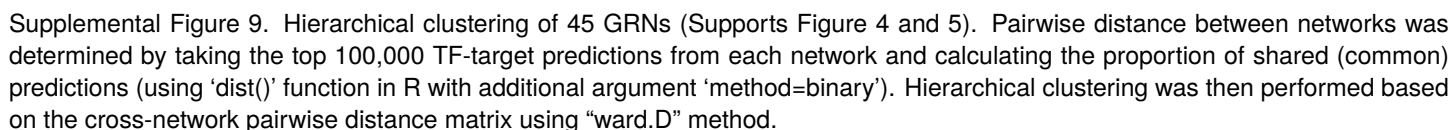


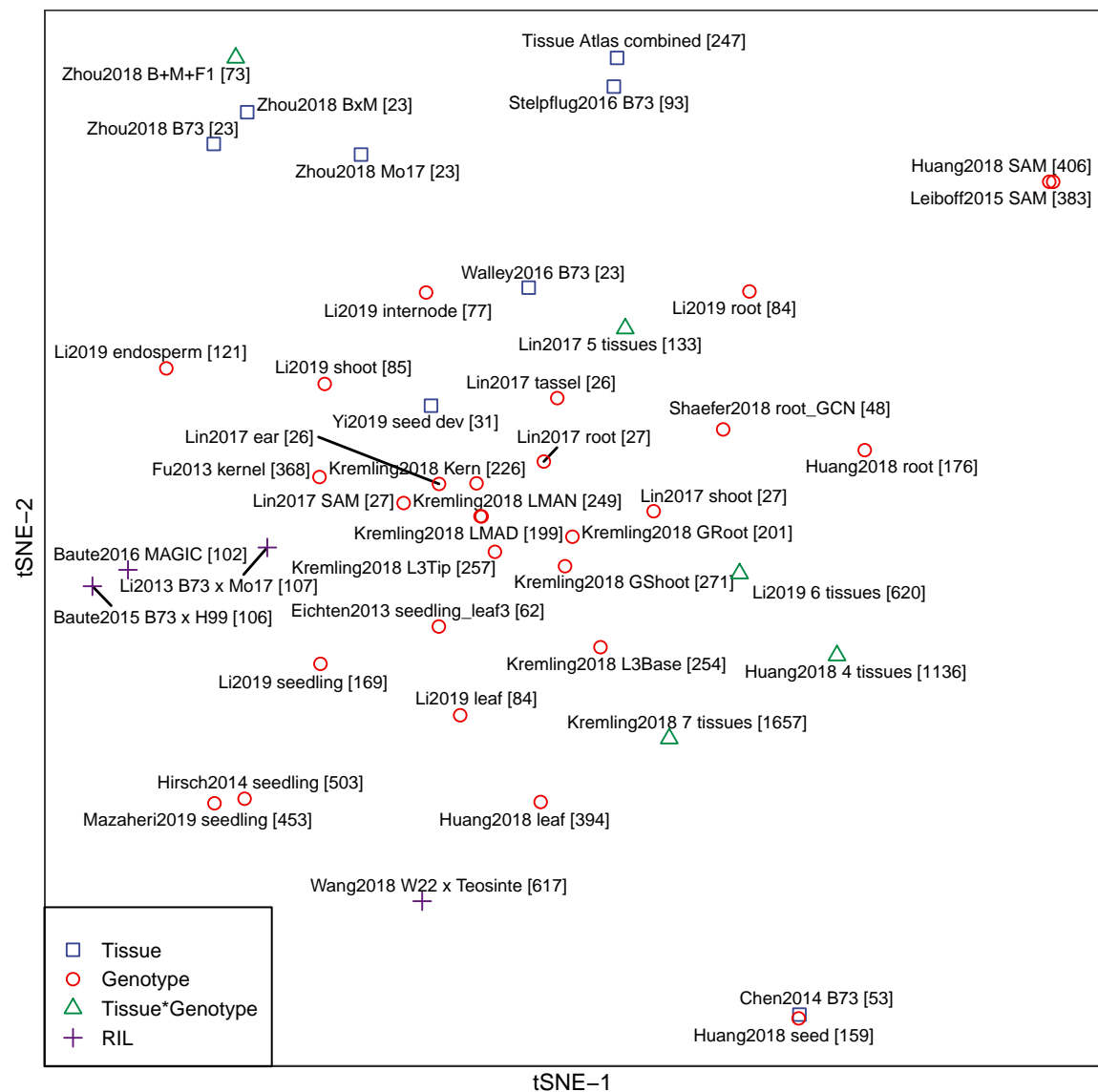
Supplemental Figure 7. Different GRNs capture distinct parts of documented transcriptional regulation interactions from Arabidopsis

for the abscisic acid (ABA) pathway and HY5 (Elongated Hypocotyl 5) regulated pathway (Supports Figure 4B and 4C).

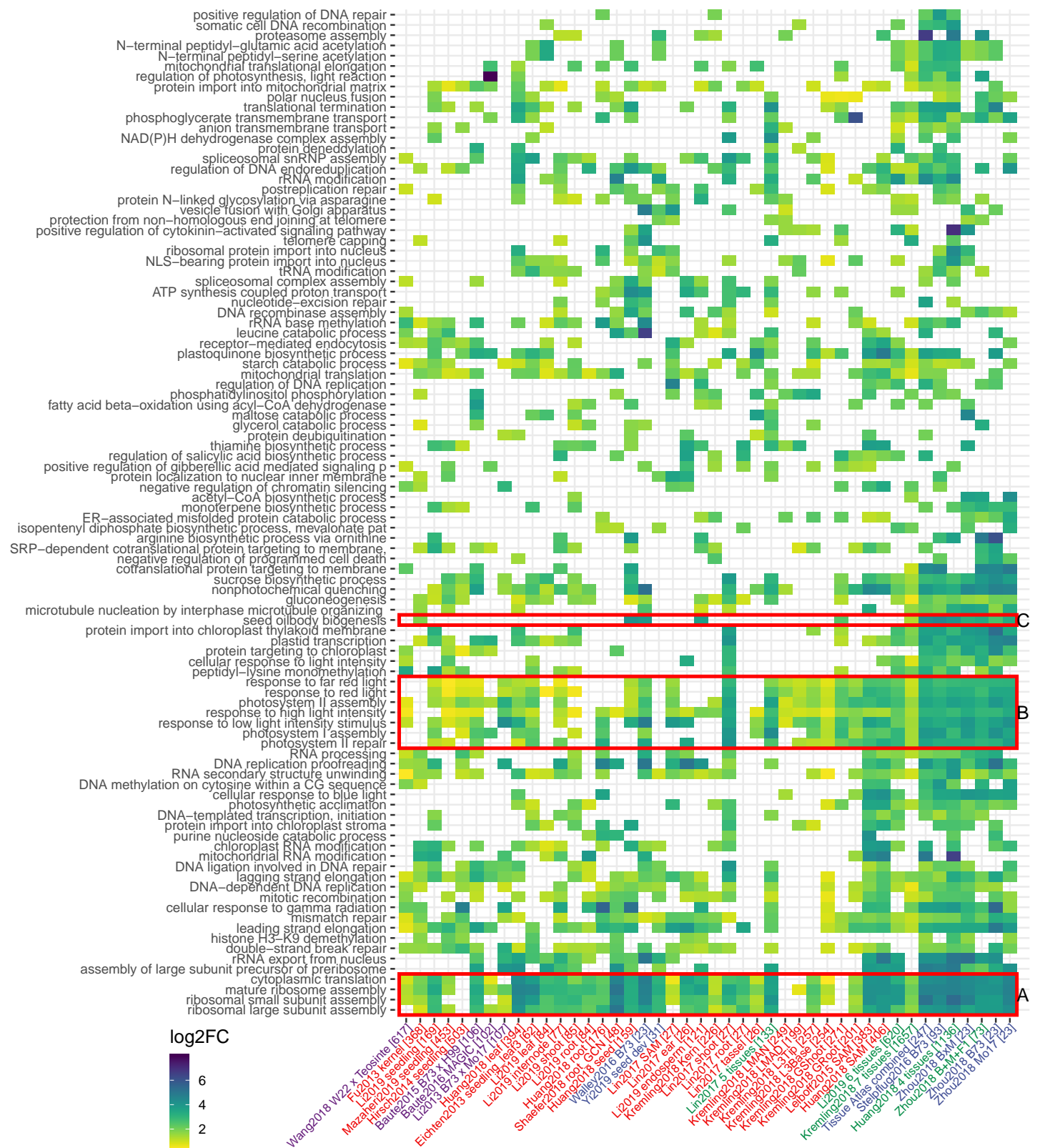


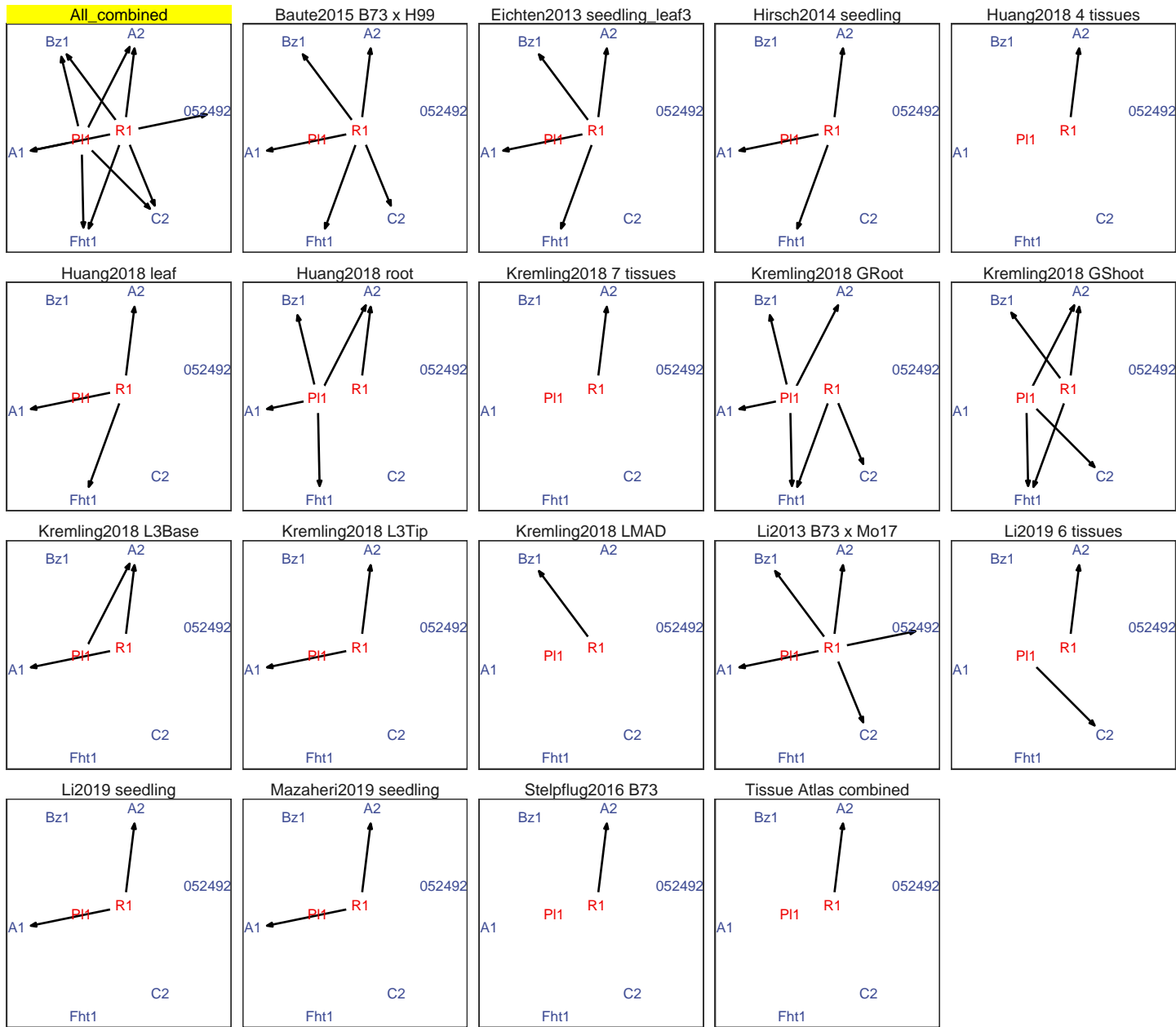
Supplemental Figure 8. Evaluation (AUROC and Wilcox P-value) of constructed GRNs using four sets of predicted TF-target interactions based on TF-binding site motif, conserved element of TFBS motif, or FunTFBS (Supports Figure 2). There are 202,670 “motif”-based predictions, 37,699 predictions based on motif and cross-species conservation, 7,459 predictions based on motif and FunTFBS as well as 4,115 predictions based on all three types of evidence.



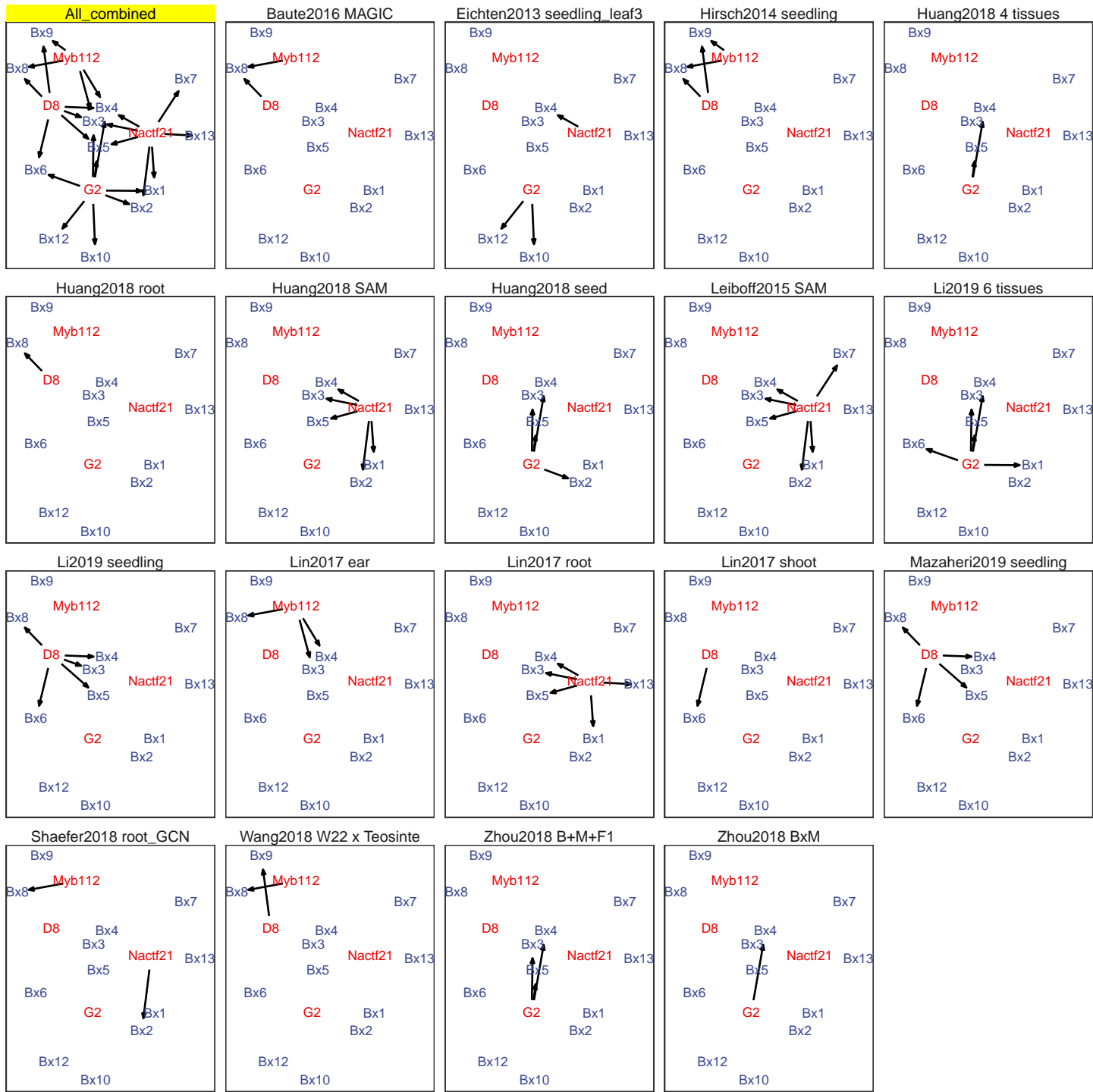


Supplemental Figure 10. T-SNE clustering of 45 GRNs (Supports Figure 4 and 5). Top 500,000 TF-target predictions were extracted from each network to perform t-SNE clustering using parameter “perplexing=9, permutation=2000”.

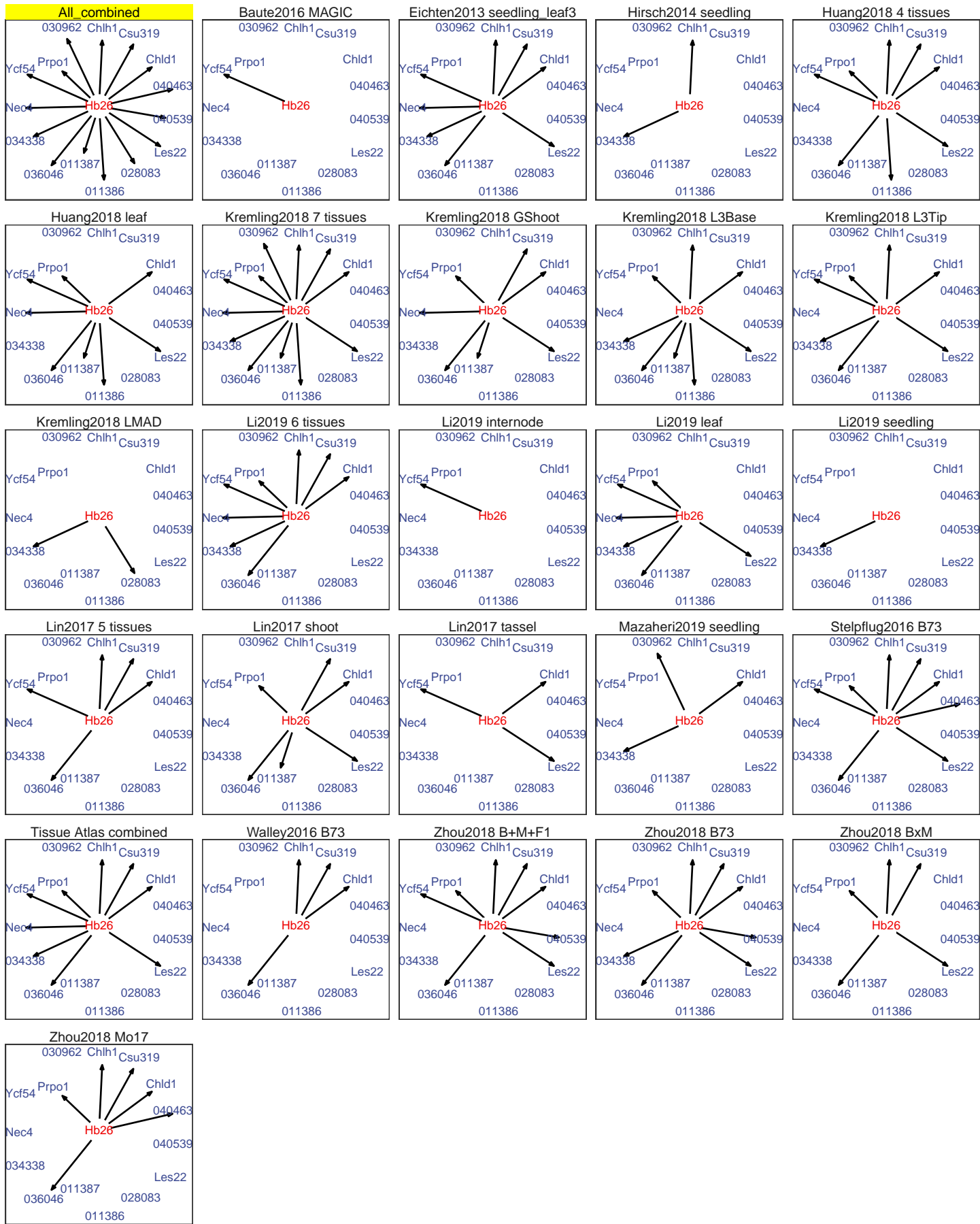




Supplemental Figure 12. Different GRNs support different parts of the anthocyanin biosynthesis pathway (Supports Figure 5).

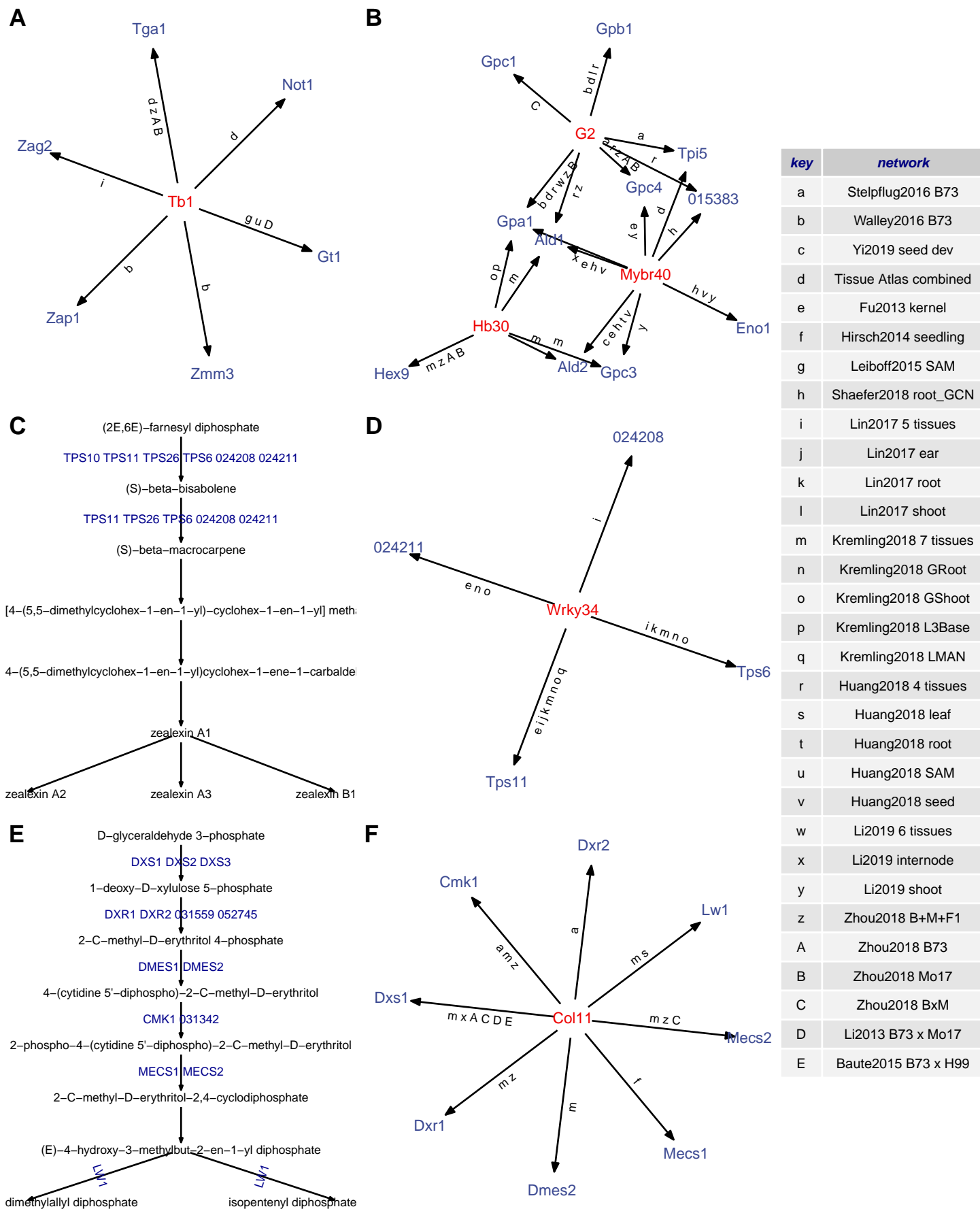


Supplemental Figure 13. Different GRNs support different parts of the DIMBOA pathway (Supports Figure 5).



Supplemental Figure 14. Different GRNs support different parts of the chlorophyllide biosynthesis pathway regulated by homeobox-

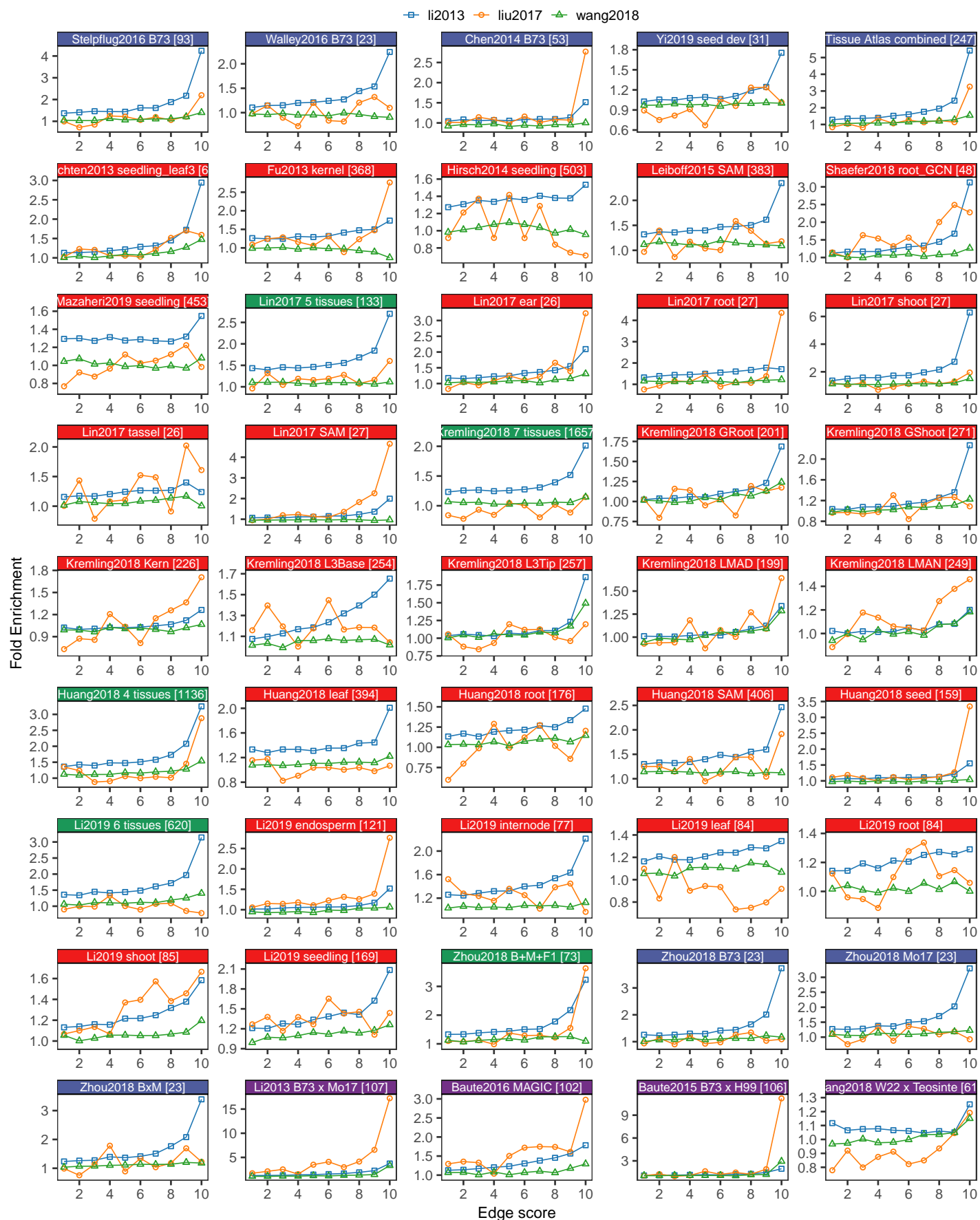
transcription factor 26 (HB26, Zm00001d008612) (Supports Figure 5).



Supplemental Figure 15. Different coexpression-based GRNs capture distinct parts of classic and CornCyc metabolic pathways

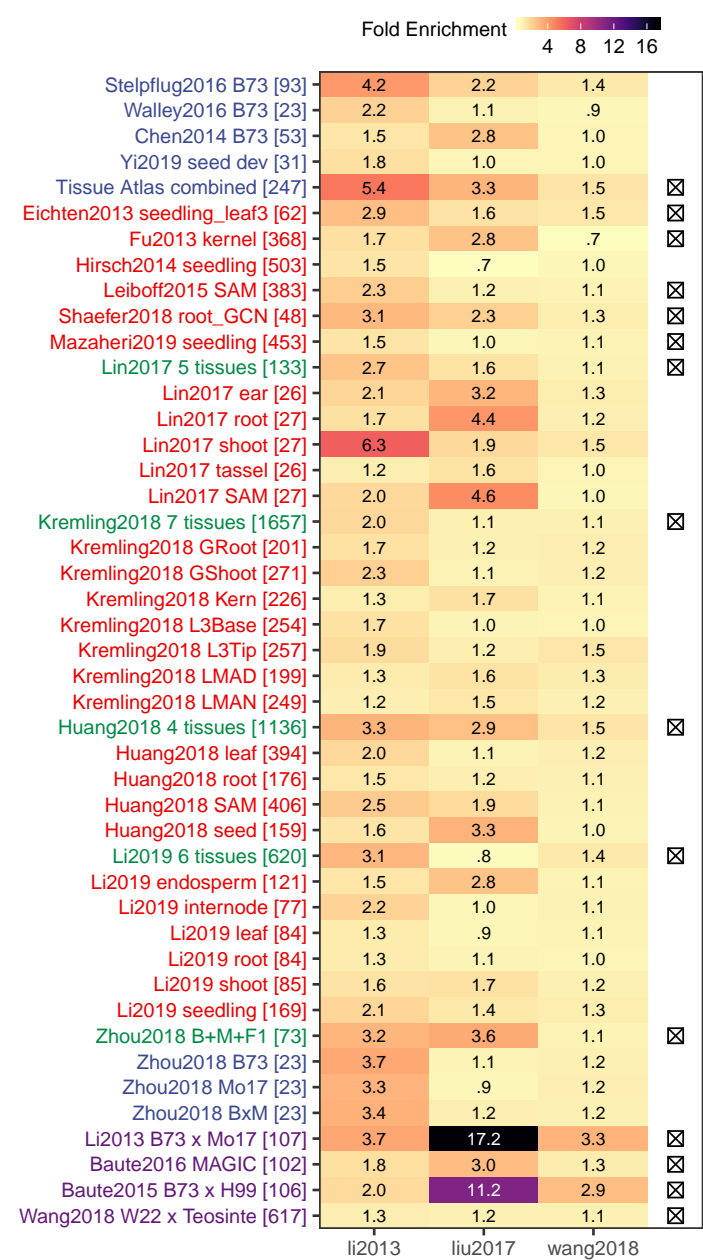
(Supports Figure 5). (A) The teosinte branched1 (tb1)-mediated pathway regulating bud dormancy and growth repression. (B) The glycolysis pathway. (C-D) The zealexin biosynthesis pathway (C) regulated by a WRKY-transcription factor 34 (WRKY34, Zm00001d009939) (D). (E-F) The methylerythritol phosphate pathway (E) regulated by a C2C2-CO-like-transcription factor 11 (COL11, Zm00001d003162) (F). The letters along the edges of the networks in (B) (D) and (F) indicate significant support from specific GRN as indicated in the key.

Supplemental Figure 16. TF-target validation of the combined tissue network in all six selected natural variation datasets (Supports Figure 6). Each panel shows the proportion of differentially expressed targets regulated by TFs showing different DE levels between two genotypes in one tissue/treatment condition. TF-target predictions were binned to 10 groups based on the interaction score in GRN. Each TF-target pair is classified according to the DE level of the TF ("non_DE", "DE1-2", "DE2-4", "DE4+" or "SPE") in each network. The proportion of TF-target pairs with the target also showing DE was then determined for each category. Within each panel the actual numbers of TF-target pairs falling into the "SPE" category (i.e., purple line) were labelled next to each point. Dashed line in each panel represents the genome-wide (background) proportion of DE genes in each tissue/treatment setting.

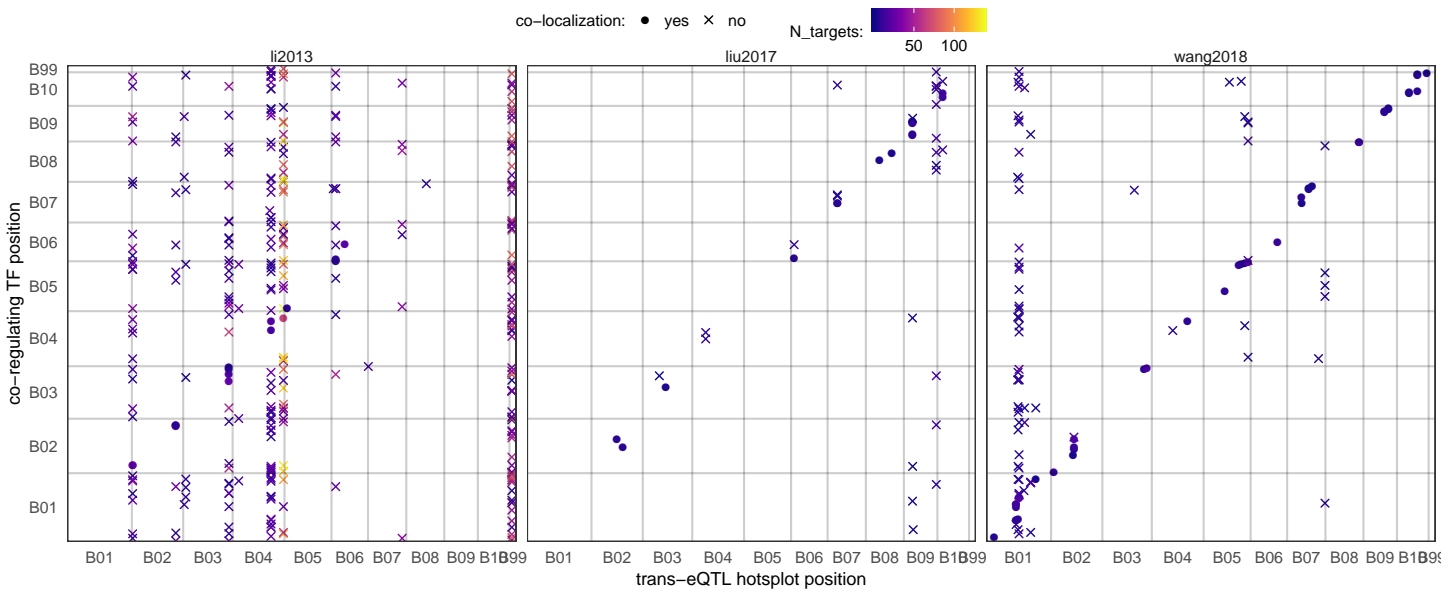


Supplemental Figure 17. Enrichment of co-regulated targets between previously identified trans-eQTL hotspots and TF-target asso-

ciations predicted by GRNs (Supports Figure 8). For each network the top 1 million TF-target predictions were binned to 10 groups based on the interaction score in GRN. Fold enrichment is determined by the same permutation approach described in Figure 2.



Supplemental Figure 18. Enrichment of co-regulated targets between previously identified trans-eQTL hotspots and TF-target associations predicted by GRNs (Supports Figure 8). For each network the top 1 million predicted TF-target associations were binned to 10 bins and only the first bin (top 100k edges) were used to assess enrichment. 15 high quality networks (marked with crosses) were selected to identify the main TF regulators underlying trans-eQTL hotspots (see Methods).



Supplemental Figure 19. Co-localization of TFs predicted by GRNs in this study and trans-eQTL hotspots identified in previous studies that regulate the same set of targets (Supports Figure 8). Each trans-eQTL hotspot were first tested for significant overlap in targets with any TFs (hypergeometric enrichment test as implemented in the phyper() function in R). To control for false positives, only TFs identified in at least two (out of 8 high quality networks, see Methods) that show significant co-regulation with at least one trans-eQTL hotspot ($p < 0.01$) were kept. Trans-eQTL hotspots identified in previous maize assemblies were lifted over to the AGPv4 assembly coordinates. Co-localization of a TF and a trans-eQTL is determined if the two coordinates are within 50-Mbp distance. Color of each dot represents the number of common targets between the predicted TF regulator and the trans-eQTL hotspot.

Supplemental Table 1. ChIP-Seq and DAP-Seq datasets used in this study.

TF alias	TF name	TF ID	Tissue	Study Type	Targets	Reference
KN1	knotted1	Zm00001d033859	ear, leaf, tassel, SAM	ChIP-seq	648	Bolduc2012
P1	pericarp color1	Zm00001d028854	endosperm	ChIP-seq	20	Morohashi2012
RA1	ramosa1	Zm00001d020430	ear	ChIP-seq	203	Eveland2014
FEA4	fascinated ear4	Zm00001d037317	ear	ChIP-seq	99	Pautler2015
HDA101	histone deacetylase homolog	Zm00001d053595	seed	ChIP-seq	112	Yang2016
O2	opaque2	Zm00001d018971	endosperm	ChIP-seq	32	Zhan2018
bZIP22	bZIP-transcription factor 22	Zm00001d021191	kernel	ChIP-seq	25	Li2018
TB1	teosinte brach1	Zm00001d033673	tiller bud	ChIP-seq	3445	Dong2019
ARF10		Zm00001d042267		DAP-seq		Galli2018
ARF13		Zm00001d049295		DAP-seq		Galli2018
ARF14		Zm00001d050781		DAP-seq		Galli2018
ARF16		Zm00001d053819		DAP-seq		Galli2018
ARF18		Zm00001d014377		DAP-seq		Galli2018
ARF25		Zm00001d011953		DAP-seq		Galli2018
ARF27		Zm00001d045026		DAP-seq		Galli2018
ARF29		Zm00001d026540		DAP-seq		Galli2018
ARF34		Zm00001d031064		DAP-seq		Galli2018
ARF35		Zm00001d014690		DAP-seq		Galli2018
ARF36		Zm00001d016838		DAP-seq		Galli2018
ARF39		Zm00001d003601		DAP-seq		Galli2018
ARF4		Zm00001d001945		DAP-seq		Galli2018
ARF7		Zm00001d039267		DAP-seq		Galli2018
BAD1		Zm00001d005737		DAP-seq		Ricci2019
BZIP25		Zm00001d010658		DAP-seq		Ricci2019
BZIP54		Zm00001d022542		DAP-seq		Ricci2019
BZIP57	FEA4	Zm00001d037317		DAP-seq		Ricci2019
BZIP72		Zm00001d008225		DAP-seq		Ricci2019
BZIP96		Zm00001d010638		DAP-seq		Ricci2019
EREB127		Zm00001d051451		DAP-seq		Ricci2019
EREB138		Zm00001d015639		DAP-seq		Ricci2019
EREB24	BBM	Zm00001d002025		DAP-seq		Ricci2019
EREB29		Zm00001d012584		DAP-seq		Ricci2019
EREB71		Zm00001d048208		DAP-seq		Ricci2019
LBD16	RA2	Zm00001d039694		DAP-seq		Ricci2019
LBD19	IG1	Zm00001d042560		DAP-seq		Ricci2019
LBD38		Zm00001d010751		DAP-seq		Ricci2019
LBD5		Zm00001d029506		DAP-seq		Ricci2019
SBP30	UB3	Zm00001d052890		DAP-seq		Ricci2019
SBP6		Zm00001d012916		DAP-seq		Ricci2019
SBP8	UB2	Zm00001d031451		DAP-seq		Ricci2019

Supplemental Table 2. TF knockout mutant RNA-Seq datasets used in this study.

TF alias	TF name	TF ID	Tissue	Reference
KN1	knotted1	Zm00001d033859	ear, leaf, tassel, SAM	Bolduc2012
P1	pericarp color1	Zm00001d028854	endosperm	Morohashi2012
RA1	ramosa1	Zm00001d020430	ear	Eveland2014
RA2	ramosa2	Zm00001d039694	ear	Eveland2014
RA3	ramosa3	Zm00001d022193	ear	Eveland2014
FEA4	fascinated ear4	Zm00001d037317	ear	Pautler2015
HDA101	histone deacetylase homolog	Zm00001d053595	seed	Yang2016
NKD1	naked endosperm1	Zm00001d002654	aleurone, endosperm	Gontarek2016
O2	opaque2	Zm00001d018971	endosperm	Zhan2018
bZIP22	bZIP-transcription factor 22	Zm00001d021191	kernel	Li2018
TB1	teosinte brach1	Zm00001d033673	tiller bud	Dong2019
GT1	grassy tillers1	Zm00001d028129	tiller bud	Dong2019

Supplemental Table 3. Natural variation datasets used for validation in this study.

author	study	condition	contrast	non-DE	DE1-2	DE2-4	DE4+	SPE
Waters2017	stress cis-trans	leaf3 cold	B73 vs B37	14,991	5,508	2,524	2,191	765
		leaf3 cold	B73 vs Oh43	13,985	6,013	2,955	2,226	800
		leaf3 control	B73 vs B37	11,868	7,131	3,468	2,551	961
		leaf3 control	B73 vs Oh43	12,804	6,395	3,213	2,545	1,022
		leaf3 heat	B73 vs B37	14,488	5,491	2,937	2,276	787
		leaf3 heat	B73 vs Oh43	13,304	5,931	3,249	2,568	927
		leaf3 cold	B73 vs Mo17	17,235	2,783	2,136	1,550	796
		leaf3 cold	B73 vs PH207	17,202	3,023	2,075	1,439	761
		leaf3 control	B73 vs Mo17	18,843	2,012	1,610	1,226	809
		leaf3 control	B73 vs PH207	19,148	1,868	1,447	1,239	798
		leaf3 heat	B73 vs Mo17	18,453	2,433	1,641	1,152	821
		leaf3 heat	B73 vs PH207	16,533	3,404	2,312	1,459	792
Marcon2017	drought stress	root control	B73 vs Mo17	13,185	6,718	2,513	1,940	651
		root drought	B73 vs Mo17	13,828	6,370	2,347	1,864	598
Sun2018	mo17 genome	bract	B73 vs Mo17	19,008	832	980	1,192	702
		endosperm	B73 vs Mo17	18,841	1,021	1,240	1,016	596
		root	B73 vs Mo17	18,760	820	1,114	1,371	649
		seedling	B73 vs Mo17	19,416	661	850	980	807
		stem	B73 vs Mo17	18,669	887	1,130	1,164	864
Zhou2018	B73 Mo17 atlas	auricle	B73 vs Mo17	14,944	3,885	2,596	2,091	860
		blade leaf	B73 vs Mo17	16,331	3,174	2,170	1,775	926
		coleoptile	B73 vs Mo17	18,653	2,392	1,389	1,367	575
		ear	B73 vs Mo17	18,838	2,425	1,213	1,095	805
		embryo	B73 vs Mo17	16,351	3,577	2,227	1,407	814
		endosperm14D	B73 vs Mo17	17,848	2,570	1,748	1,468	742
		endosperm27D	B73 vs Mo17	16,695	3,105	2,254	1,458	864
		flag leaf	B73 vs Mo17	16,090	3,146	2,329	1,898	913
		floret	B73 vs Mo17	17,037	3,259	1,977	1,342	761
		husk	B73 vs Mo17	16,723	3,362	1,809	1,605	877
		internode	B73 vs Mo17	13,644	4,273	2,844	2,653	962
		kernel	B73 vs Mo17	17,590	2,946	1,734	1,362	744
		radicle root	B73 vs Mo17	18,120	2,346	1,764	1,501	645
		root	B73 vs Mo17	17,334	2,883	1,844	1,499	816
		seed imbibed	B73 vs Mo17	12,068	5,342	3,606	2,626	734
		seedling leaf	B73 vs Mo17	16,245	2,938	2,286	2,079	828
		seedling meristem	B73 vs Mo17	19,207	1,923	1,249	1,235	762
		seedling root	B73 vs Mo17	18,842	2,009	1,631	1,180	714
		sheath	B73 vs Mo17	15,209	3,885	2,633	1,810	839
		silk	B73 vs Mo17	15,378	3,577	2,303	2,152	966
		spikelet	B73 vs Mo17	17,984	2,736	1,589	1,209	858
		tassel	B73 vs Mo17	15,594	3,856	2,435	1,677	814
		tassel stem	B73 vs Mo17	12,564	4,625	3,512	2,652	1,023